Characterization of Molecular Scale Environments in Polymer Films by Single Molecule Spectroscopy

Yanwen Hou, Angela M. Bardo, Cruz Martinez, and Daniel A. Higgins*

Department of Chemistry, Kansas State University, Manhattan, Kansas 66506-3701

Received: July 9, 1999; In Final Form: November 2, 1999

Single molecule spectroscopic methods are used to obtain detailed information on the polarity and rigidity of molecular-scale environments found in thin poly(vinyl alcohol) (PVA) and poly(methyl methacrylate) (PMMA) films. Nile Red is employed as a highly sensitive spectroscopic probe of environmental properties in these experiments. Fluorescence spectra are recorded for numerous single molecules and their peak positions and widths determined by fitting the spectra to Gaussian functions. The spectral data are analyzed using a new model for the dependence of the Nile Red charge-transfer transition on the properties of the surrounding medium. This model is based on previous work by Marcus (Marcus, R. A. *J. Phys. Chem.* **1990**, *94*, 4963). Additional information required for the analysis is obtained from extensive bulk solution-phase absorption and fluorescence studies. A broad inhomogeneous distribution of environments is found for PVA. The results are shown to depend significantly on PVA film water content, with the results for hydrated films indicating the presence of less rigid environments. In contrast to the PVA results, two distinct classes of environments are found in the PMMA films. On the basis of an analysis of the data using the aforementioned model, it is concluded that the two environments differ in rigidity but have nearly identical polarity.

I. Introduction

Fluorescence-based chemical sensors are now being developed for detection of metal ions, proteins, organic and inorganic pollutants and poisons, and other biologically active compounds.[1−4] In many of these devices, the presence of an analyte is observed via changes in the fluorescence characteristics of dye dopants and/or complexing agents entrapped within solid polymeric supports. The sensing event often results from a chemical reaction, electron transfer, or energy transfer between the analyte and dopant. The choice of dopant is, therefore, of obvious importance in the production of efficient and selective sensors. However, appropriate dopant selection requires detailed prior knowledge of dopant and analyte properties in the specific medium in which they are to be used. It is indeed well-known that the electronic properties of polar dye molecules proposed for use in chemical sensors are highly dependent on the polarity of the surrounding medium (or solvent). As a result, significant effort has been devoted to developing methods and models for determining the polarity of environments found in liquid and solid systems.[5−13] To date, much of this work has been performed using bulk spectroscopic methods, which have provided information on the average properties of these materials. However, solid polymer films are often highly inhomogeneous. The average properties determined by bulk methods then only reflect the nature of a small subset of environments actually present. Such methods therefore do not provide enough detailed information to fully understand and optimize the chemistry occurring in sensor devices.

Single molecule spectroscopic methods promise to provide detailed new information on the distribution of environments present within such materials and, hence, overcome some of these limitations.[14] Early demonstrations of optical single molecule detection have provided the basis for such studies.[15−21] Both spatial[22,23] and temporal[17,24] variations in local environmental properties have been observed via spatial and temporal variations in single molecule fluorescence spectra. Discrete photochemical events such as permanent bleaching and triplet blinking, both of which are sensitive to the surrounding environment, have also been studied.[25−29] Dynamic events such as single molecule rotation and translation have also been monitored and related to film properties.[30−34] With the advances in experimental methods and fundamental understanding of single molecule phenomena provided by these studies, single molecule experiments are now being performed for the sole purpose of gaining a better understanding of thin film materials[35] and surfaces.[36] Recently, we have used single molecule spectroscopic methods to characterize the distribution of molecular-scale environments within dye-doped silicate glass films prepared by the sol−gel process.[35] We demonstrated that static single molecule spectroscopy and observation of single molecule fluorescence "switching" could be employed to observe spatial and temporal variations in local silicate properties.

In the current study, a much more quantitative analysis of the environments found in thin films of organic polymers is presented. These studies employ the dye Nile Red (structure shown in Figure 1) as a highly sensitive spectroscopic probe of poly(methyl methacrylate) (PMMA) and poly(vinyl alcohol) (PVA) thin films. An extension of the models for the solvent dependence of charge-transfer spectra developed by Marcus[37−39] and others[12,13,40−44] is presented and used in the analysis of the single molecule spectroscopic data. Using additional data obtained from extensive studies of the bulk solution phase spectra of Nile Red provides detailed information that reflects both the "static" (polarity) and "dynamic" (rigidity/fluidity) properties of the individual local environments and their distributions. The methods and results presented here promise to yield valuable new insight into the distribution of environments found in solid thin film materials.

II. Theoretical Background

The solvent dependence of charge transfer spectra for polar solutes in liquid solvents has been described previously in detail.[12,13,37−39,44] Briefly, the absorption and fluorescence transition energies, $\bar{\nu}_{abs}$ and $\bar{\nu}_{fl}$ (in cm^{-1}) for such spectra are

10.1021/jp992312y CCC: $19.00
Published on Web 12/23/1999

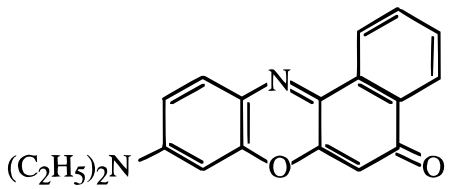

Figure 1. Chemical structure of Nile Red.

related to the free energy, $\Delta G°$, of the transition, the solvent reorganization energy λ_o, and the internal molecular reorganization energy λ_i of the solute as follows:[38,44]

$$\bar{\nu}_{abs} = \Delta G° + \lambda_o + \lambda_i \qquad \bar{\nu}_{fl} = \Delta G° - \lambda_o - \lambda_i \quad (1a,b)$$

Equations 1a and b are usually applied to broad, structureless spectra. In the present work, $\bar{\nu}_{abs}$ and $\bar{\nu}_{fl}$ are taken as the origin of the vibronic progression (i.e., the 0−0 transition energy) observed in solution-phase spectra of Nile Red. In this case, λ_i represents the reorganization energy associated with the low-frequency modes of this particular vibronic transition. This definition of λ_i differs from previous theories[38,44] and allows for better modeling of the often-resolved vibronic structure of the single molecule spectra. The above model assumes that the solvent behaves as a structureless continuum and neglects specific solute−solvent interactions. In this case, λ_o (or the orientation polarizability, Δf) is related through dielectric continuum theory to the solvent's static, ϵ, and optical, η^2, dielectric constants by

$$\lambda_o = \frac{(\Delta\mu)^2}{hca^3}\left[\frac{\epsilon - 1}{2\epsilon + 1} - \frac{\eta^2 - 1}{2\eta^2 + 1}\right] = \frac{(\Delta\mu)^2}{hca^3}\Delta f \qquad (2)$$

In eq 2, $(\Delta\mu)^2 = (\mu_e - \mu_g)^2$ and μ_g and μ_e are the solute's ground and excited-state dipole moments, a is the radius of the spherical cavity in which the solute resides. Equation 2 describes the change in energy of the solute−solvent system resulting from relaxation of the solvent dipoles following a change in the solute's dipole moment (due to an electronic transition). The free energy of the electronic transition is also dependent on the solvent properties and is given by[44]

$$\Delta G° = \Delta G°_v - \Delta\Delta G° = \Delta G°_v - \frac{\Delta(\mu^2)}{hca^3}\left[\frac{\epsilon - 1}{2\epsilon + 1}\right] \qquad (3)$$

where $\Delta G°_v$ is the free energy of the transition in a vacuum, $\Delta(\mu^2) = \mu_e^2 - \mu_g^2$ and $\Delta\Delta G°$ describes the solvent-dependent part of the free energy. As a result of their dependence on solvent properties, both $\Delta G°$ (or $\Delta\Delta G°$) and λ_o may be used as semiquantitative measures of the properties (associated with the polarity) of specific liquid solvent systems. Indeed, Δf and λ_o have been used extensively in this manner.[9,10,12,13,45]

For solid systems such as those studied here, this model must be modified to appropriately describe the influence of the surrounding environment on the spectra. The differences between solid- and liquid-phase environments are reflected most dramatically in the blue-shifted fluorescence usually observed for solutes in frozen solvents.[45,46] Wrighton et al. have appropriately named this phenomenon "rigidochromism",[46] as it results from the restriction of solvent dipole motions. To account for such effects, λ_o is divided into two components: (i) a "static" component that describes the contribution of the orientationally frozen dipoles to the transition energy and (ii) a "dynamic" component that describes solvent dipole relaxation similar to that in liquids. These two components are designated λ_{oo} and λ_{oi}, respectively, yielding[39]

$$\bar{\nu}_{abs} = \Delta G° + \lambda_{oo} + \lambda_{oi} + \lambda_i$$
$$\bar{\nu}_{fl} = \Delta G° + \lambda_{oo} - \lambda_{oi} - \lambda_i \quad (4a,b)$$

Equations 4a and b cannot be directly applied in the single molecule studies of polymer films presented here because they describe samples prepared under different conditions. These equations are valid for samples prepared by slowly cooling a liquid solution below its freezing point. Under such circumstances, the frozen solvent configuration is assumed to be the equilibrium configuration surrounding the ground-state solute. This assumption is no longer valid in the present experiments for several reasons. First, the polymer films studied here were prepared in advance, in the absence of dye. Therefore, the film properties are determined by the polymer alone, as desired, and are likely different from those of films prepared from dye-doped polymer solutions. Furthermore, the films were prepared by spin casting, with associated rapid solvent evaporation. Polymer chain organization under such conditions is likely far different from that of films prepared by slowly cooling polymer melts. Finally, the equilibrium configuration referred to in the model of eqs 4a,b most appropriately describes the average properties of a bulk sample. The spontaneous fluctuations in the solvent configuration that occur in all samples are averaged out in bulk experiments. They do, however, contribute to the observed spectral width (inhomogeneous broadening). In the present experiments, these nonequilibrium configurations are frozen into the sample and are directly observed. As a result, the environmental properties are expected to be highly variable and possibly far from the equilibrium configuration expected under more ideal circumstances.

In single molecule (i.e., local) studies, both the ground- and excited-state energies are altered by the nonequilibrium configuration. That is, with the primed parameters (λ'_{oo}, λ'_{oi}, and λ_i') representing the parameters for the excited state, eqs 4a,b become

$$\bar{\nu}_{abs} = \Delta G° + \lambda'_{oo} - \lambda_{oo} + \lambda'_{oi} + \lambda'_i \approx \Delta G° + \lambda_{oi} + \lambda_i \quad (5a)$$
$$\bar{\nu}_{fl} = \Delta G° + \lambda'_{oo} - \lambda_{oo} - \lambda_{oi} - \lambda_i \approx \Delta G° - \lambda_{oi} - \lambda_i \quad (5b)$$

The ground- and excited-state reorganization energies are likely somewhat different; however, as in the past,[44] it is assumed that they are approximately equal. The contributions of the frozen dipoles to the transition energy (λ_{oo} and λ'_{oo}) then drop out of the equations, as shown in the approximate expressions given on the right side of eqs. 5a,b. Note that eqs 5a,b differ from previous models[39] in that they imply simultaneous blue and red shifts in the solid-state fluorescence and absorption spectra, respectively, relative to a liquid environment of otherwise similar properties.

As in liquid solvents, the parameters $\Delta G°$ (or $\Delta\Delta G°$) and λ_{oi} may then be used as a means to characterize the properties of the local environments found within solid films. Since $\Delta G°$ is the transition energy after complete relaxation of the environmental dipoles, it is interpreted here to describe the static polarity of the local environment. λ_{oi} is the energy associated with relaxation of the solute−solvent system during the excited-state lifetime. Therefore, it may be interpreted as a measure of environmental "rigidity". It also depends on polarity, with λ_{oi} expected to take on smaller values in less polar environments, based on a continuum model. In bulk spectroscopic studies, λ_{oi} is usually obtained by measuring the Stokes shift between absorption and fluorescence.[39] However, in single molecule studies, only the fluorescence spectrum can be measured. No direct information on the Stokes shift is available. In this case,

the widths of the single molecule fluorescence spectra may be used to obtain the additional information required. Here, the full-width-at-half-maximum (fwhm), $\delta\bar{\nu}_{fl}$, of a single vibronic band is employed. Broadening by the low-frequency intramolecular vibrational modes associated with a single vibronic band is treated classically,[44] giving

$$\delta\bar{\nu}_{fl}(\text{solid}) \approx 4((\lambda_{oi} + \lambda_i)(\ln 2)kT)^{1/2} \quad (6)$$

where k is the Boltzmann constant and T is temperature.

For spectra from solid samples, the validity of eq 6 depends on the same assumptions as its liquid-state analogue.[37,38,44] Specifically, the spectral width must be dominated by solvent and intramolecular motions, rather than static inhomogeneity (i.e., variations in $\Delta G°$). In bulk room temperature spectroscopic studies of solids, it is likely that the width of the emission band is actually dominated by sample inhomogeneity. Little information on environmental properties can be obtained under such circumstances. Single molecule methods, however, provide a distinct advantage in that static inhomogeneity does not contribute to the spectral width. Rather, it contributes only to variations in the peak positions of the individual single molecule spectra. The widths of single molecule spectra then provide direct information on the total reorganization energy (i.e., $\lambda_i + \lambda_{oi}$).

It should be noted that environmental variations that occur on time scales greater than the excited-state lifetime (nominally 10 ns) but less than the time scale of the experiment (a few seconds) will also contribute to the single molecule spectral widths, a phenomenon known as "spectral diffusion."[17,24,47] Its contributions are neglected in the above model and are believed to be of secondary importance. Such an assumption is supported both by previously published low-temperature[17,47] and room temperature[24] studies of spectral diffusion, as well as by experimental results given below.

Again, the spectral width only provides information on the sum of λ_{oi} and λ_i. Additional information at the single molecule level is therefore required to strictly separate the two contributions to the reorganization energy. Since λ_i likely varies to a certain extent, as evidenced by recently published results showing variations in the vibronic band structure of single molecule spectra,[26] such information is particularly important. Presently, there are no additional experiments known that can provide this information. Therefore, for the purposes of this publication, it is simply noted that both parameters in fact provide the desired measure of environmental rigidity, albeit by different mechanisms. That is, rigid environments that "freeze-out" certain molecular motions also lead to small values of λ_i. However, since the dye employed here was selected for its dramatic solvent sensitivity, and since it has a highly rigid structure (and therefore, relatively few low-frequency modes) it is assumed that any variations in spectral width observed will be dominated by variations in λ_{oi}. As a first approximation, the value of λ_i is then taken to be a constant, independent of local environment, and its value is determined from bulk liquid-phase spectra.

Finally, $\Delta\Delta G°$ ($=\Delta G°_v - \Delta G°$) is the static polarity parameter that actually depends on the environmental properties. Its determination requires prior knowledge of $\Delta G°_v$. As in the case of λ_i, $\Delta G°_v$ is determined from bulk liquid-phase absorption and fluorescence spectra recorded in different solvents. Plots of the peak positions of the spectra versus the relevant solvent parameters (eqs 2 and 3) are fit to eqs 1a,b to determine both λ_i and $\Delta G°_v$.

III. Experimental Considerations

A. Samples. The polymer films employed were prepared by spin casting dilute solutions onto clean glass microscope coverslips. Poly(methyl methacrylate), poly(vinyl alcohol), and the dye were all obtained from Aldrich and were used as received. PMMA films were prepared from methylene chloride solution, while PVA films were prepared from aqueous solution. The resulting films were a few hundred nanometers in thickness. Methanolic Nile Red solution (0.1−5 nM) was subsequently spin cast on top of the preformed polymer films. It is expected that the dye molecules migrate into the polymer films during spin casting. All organic solvents employed were spectrophotometric grade. Aqueous solutions were prepared from Millipore-filtered water. To investigate the effects of residual solvent on the spectra, the films were either used immediately following preparation or were dried one to 2 days in the ambient environment (PMMA samples) or dried for several hours under a nitrogen atmosphere (PVA samples).

B. Instrumentation. A sample scanning confocal microscope was employed in these studies and has been described previously.[35] Briefly, the sample scanning stage (Queensgate) incorporates closed-loop X,Y feedback for accurate determination of the location of each molecule in imaging experiments. The sample and stage were mounted on an inverted, epi-illumination microscope (Nikon). The 514.5 nm line of an argon ion laser was used to excite the Nile Red molecules. The power into the microscope was typically maintained at 200−400 nW. A 100×, 1.3 numerical aperture objective was used to produce a nearly diffraction-limited focused laser spot of ≈300 nm diameter on the sample and to collect the fluorescence emitted by the molecules. Appropriate notch (Kaiser Optical) and long-pass filters were used to isolate the fluorescence from the excitation light. A single photon counting avalanche diode, positioned in a secondary image plane of the microscope, was used to detect the fluorescence in imaging experiments. This same configuration was used to record the time-dependent, spectrally integrated fluorescence signal from individual molecules. Single molecule fluorescence spectra were recorded using a 0.3 m imaging spectrograph (Acton Research) and associated liquid N_2-cooled CCD array detector (Princeton Instruments). In the majority of experiments, the spectra were recorded by integrating the dispersed fluorescence from each molecule for 10−15 s. In experiments performed to determine the approximate contribution of spectral diffusion to the observed spectral widths, the fluorescence was integrated for 0.25 s. Bulk fluorescence spectra of Nile Red in the solid films and in solution were recorded using a commercial spectrofluorometer (SPEX Fluoromax-2).

IV. Results and Discussion

A. Determination of Spectroscopic Parameters for Nile Red. The dramatic solvent/environmental sensitivity of Nile Red is demonstrated in the solution-phase spectroscopic data presented in Figure 2. As shown, $\bar{\nu}_{abs}$ and $\bar{\nu}_{fl}$ simultaneously shift from 19 600 to 17 700 cm^{-1} and 19 000 to 15 800 cm^{-1}, respectively, between *n*-hexane and methanol solutions. The Stokes shift between absorption and fluorescence ranges from a minimum of 600 cm^{-1} in hexane to a maximum of 1900 cm^{-1} in methanol. The transition energies were determined by fitting the spectra to a series of Gaussian functions. Again, only the 0−0 transition energy of the dominant high-frequency vibrational mode is reported. The fits to the spectra indicate this band is largest in all but hexane solution. These data are used for determination of the solute parameters $\Delta G°_v$ and λ_i below.

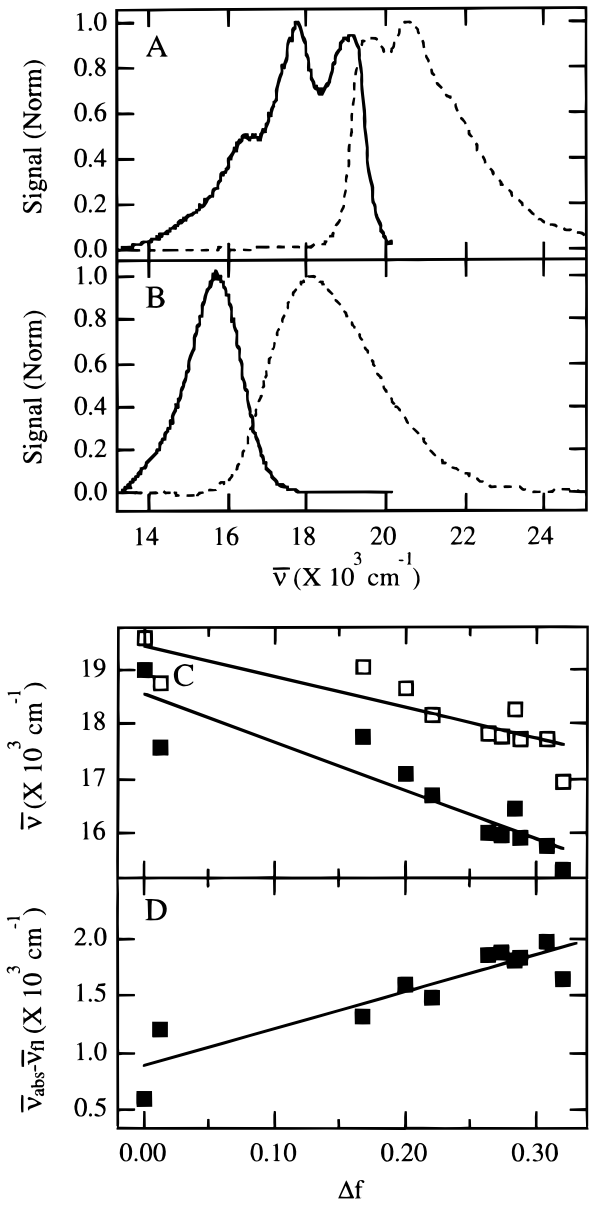

Figure 2. Bulk absorption and fluorescence spectral data for a number of solvents. (A,B) Absorption (- - -) and fluorescence (—) spectra in *n*-hexane and methanol, respectively. (C) Absorption (open squares) and fluorescence (filled squares) peaks ($\bar{\nu}_{abs}$ and $\bar{\nu}_{fl}$) plotted versus solvent orientation polarizability (Δf). The solvents used are (from left to right on the plot) *n*-hexane, toluene, diethyl ether, ethyl acetate, methylene chloride, 1-butanol, 1-propanol, acetone, ethanol, methanol, and water. (D) Stokes shift data plotted versus Δf. The data show the dramatic sensitivity of the Nile Red emission maximum and bandwidth to solvent properties.

The solvent sensitivity of Nile Red results from the large increase in dipole moment that occurs upon excitation to the lowest excited state (a charge-transfer transition). Pople−Pariser−Parr (PPP) π-electron calculations[48−51] have been used to predict the transition energy, transition dipole, and change in dipole moment for this transition. Figure 3 shows these results. As has been shown previously for similar dye molecules,[52] two excited states are possible in Nile Red, depending on the specific orientation of the pendant diethylamine group relative to the ring structure. The planar configuration ($\phi = 0°$ in Figure 3; amine group conjugated to the ring) yields a higher energy excited state that is highly fluorescent; a value for $\Delta\mu$ of 11.6 D is predicted by the PPP method. Rotation of the amine group by 90° ($\phi = 90°$) from this orientation yields a much lower energy, nonfluorescent (or weakly fluorescent) excited

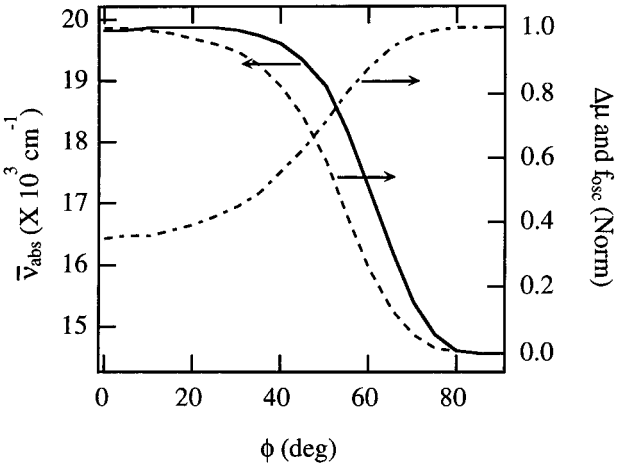

Figure 3. Results of PPP π-electron calculations for Nile Red. Plotted are the predicted transition energy $\bar{\nu}_{abs}$ (—), relative change in dipole moment $\Delta\mu$ (—·—), and relative oscillator strength, f_{osc} (- - -) as a function of the diethylamine group rotation angle ϕ. $\phi = 0°$ when the diethyl groups are in the plane of the ring. Rotation of the amine group was simulated by varying the bond resonance energy parameter in the PPP calculations.

state with a much larger $\Delta\mu$ (see Figure 3). These two states have been classified as internal charge transfer (ICT) and twisted ICT (TICT) states, respectively.[10,52−54] For these calculations, adjustments to the bond resonance energies (a PPP method parameter) were made to simulate amine group rotation. All solvent effects were neglected. Qualitatively, these results suggest that in nonpolar environments, the less polar ICT state is favored and the molecule should be highly fluorescent. In more polar media, the much larger TICT dipole is stabilized and the molecule should become less fluorescent. Previously published quantum yield measurements for Nile Red have already demonstrated these effects.[53] Spectral shifts larger than those expected from variations in solvent dielectric properties alone (e.g., as given in eqs 2 and 3) are also predicted by the present results. That is, both variations in $(\Delta\mu)^2$ and $\Delta(\mu^2)$ also contribute to the solvent sensitivity of the Nile Red spectra (see Figure 2).

Values for ΔG_v° and λ_i are obtained by fitting at least two of the three curves $\bar{\nu}_{abs}$, $\bar{\nu}_{fl}$, and $\bar{\nu}_{abs} - \bar{\nu}_{fl}$ shown in Figure 2 (fits not shown) to the parameters given in eqs 1−3. Specifically, the intercepts (where ϵ and η^2 both tend to one) of the fitted data provide these values. Note that although $(\Delta\mu)^2$ and $\Delta(\mu)^2$ are expected to vary with solvent, they are assumed constant for the fitting procedure. Relatively little error in $\Delta G°$ and λ_i should result from this assumption since only the intercepts are used. From the fit of the Stokes shift data, $2\lambda_i$ is obtained, giving $\lambda_i = 400 \pm 100$ cm^{-1}. The intercepts of the fitted $\bar{\nu}_{abs}$ and $\bar{\nu}_{fl}$ plots yield $\Delta G_v^\circ \pm \lambda_i$, giving $\Delta G_v^\circ = 20600$ cm^{-1}. The slopes of the $\bar{\nu}_{abs}$ and $\bar{\nu}_{fl}$ fits also give estimates for $\Delta(\mu^2)$/hca^3 and $(\Delta\mu)^2$/hca^3, assuming they are constant. These values are determined to be 7900 and 1900 cm^{-1}, respectively, giving estimates for μ_g and μ_e of 11.0 and 17.8 D, when a is taken to be 5 Å These values are similar to those reported in previous studies[54,55] and most accurately reflect the properties of the molecule in nonpolar environments.

Spectral widths measured in nonpolar bulk solutions also provide a means for estimating λ_i. For this determination, the fluorescence spectrum in hexane was fit to a series of Gaussians, giving a vibronic band spacing of 1300 cm^{-1}. The width of the highest energy vibronic band is determined to be 650 cm^{-1} (fwhm), yielding $\lambda_i \approx 500$ cm^{-1} (from the liquid-phase analogue of eq 6). Note that this value is smaller than that typically

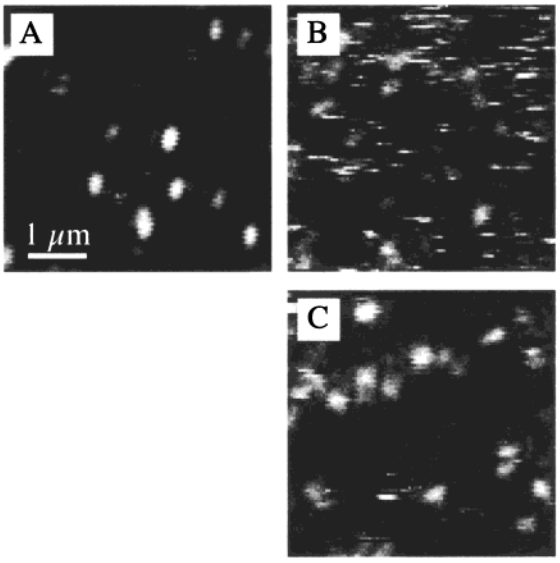

Figure 4. Fluorescence images of (A) PMMA and (B,C) PVA films doped with Nile Red. The images presented in (A) and (B) were recorded under ambient conditions. That shown in (C) was recorded in a nitrogen environment (the sample had been kept under nitrogen for several hours). Images B and C were recorded using the same sample.

reported for other molecules,[38] because it is associated with only the low-frequency intramolecular modes. The actual value used in the analysis of the single molecule data was determined from the minimum widths observed for the single molecule spectra.

B. Single Molecule Studies of Polymer Films. For characterization of local environments in PMMA and PVA, individual Nile Red molecules were first located by sample-scanning confocal imaging methods. Typical fluorescence images are shown in Figure 4. The background count rate in these images is on the order of 30 counts/pixel. The signal at each pixel was integrated for 40 ms. Both the PMMA sample and the PVA sample dried and imaged under nitrogen show several round fluorescent spots in their respective images. These spots result from fluorescence emission by individual Nile Red molecules. Conclusive proof that emission from single molecules produced these spots is obtained from a number of standard observations.[18] As shown previously,[35] the vast majority of spots, and hence the associated molecules, appeared to remain at fixed locations (to within ±30 nm).

Once spatially located, fluorescence spectra for the individual molecules were recorded. Examples of the spectra obtained are shown in Figure 5. These spectra have been selected to show the wide range of positions, widths, and shapes observed, qualitatively depicting the range of environments present within these films. Bulk spectra for the films are also shown in Figure 5 for comparison purposes. Distributions representing the range of environments found in PMMA and PVA were compiled from numerous single molecule spectra like those shown here. Specifically, histograms of $\bar{\nu}_{fl}$, $\delta\bar{\nu}_{fl}$, $\Delta\Delta G°$, and λ_{oi} were constructed from the data; the results are plotted in Figures 6 and 7. The values for $\bar{\nu}_{fl}$ and $\delta\bar{\nu}_{fl}$ were obtained by fitting the blue edge and peak of each spectrum to a single Gaussian. The red edge was excluded from the fits because of variability in the vibronic band progression. Again, $\Delta\Delta G°$ represents the shift in the transition energy determined by the static properties of the local environment. A value for λ_i of 250 cm^{-1} was used to calculate $\Delta\Delta G°$, and λ_{oi} from the $\bar{\nu}_{fl}$ and $\delta\bar{\nu}_{fl}$ data. The larger values for λ_i estimated from the solution phase data could not be used to fit the narrowest single molecule spectra. This likely results from differences in λ_i for the different molecules; such

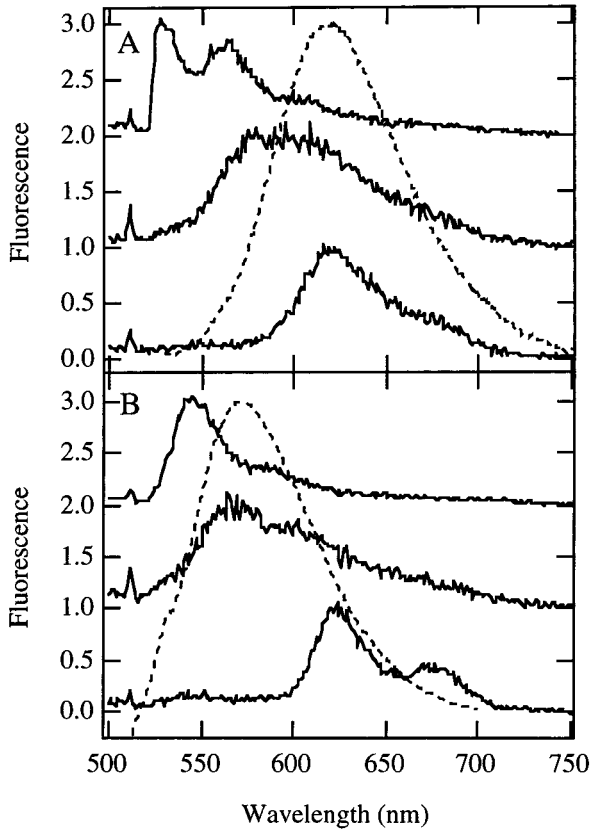

Figure 5. Example single molecule fluorescence spectra (—) and bulk spectra (- - -) for Nile Red in (A) PVA and (B) PMMA films. The data show the dramatic spectral variations observed between individual molecules.

variations are neglected in the present study for the reasons mentioned above. The smaller λ_i value does, however, fall approximately within the error limits associated with determining λ_i from the Stokes shift data (see above).

Several observations may be made directly from the spectroscopic data ($\bar{\nu}_{fl}$ and $\delta\bar{\nu}_{fl}$ histograms). First, both histograms for the PMMA samples (see Figure 6) clearly show two distinct peaks in their respective distributions. In contrast, both histograms for PVA (dried film data, see Figure 7) exhibit single-peaked distributions. These results suggest that two distinct "classes" of environments exist in the PMMA films. However, the exact nature of these environments cannot be deduced from these data alone.

A more complete understanding of the origins of the two peaks in the PMMA data is obtained using the theory presented in eqs 1−6. The $\Delta\Delta G°$ and λ_{oi} distributions calculated using this theory are presented in Figure 6 and provide the necessary additional information. The $\Delta\Delta G°$ data for PMMA clearly shows a single peak in its distribution. Again, $\Delta\Delta G°$ represents a measure of the static polarity of each environment. This result suggests the two types of environments reflected in the $\bar{\nu}_{fl}$ and $\delta\bar{\nu}_{fl}$ data have similar polarities. If the two peaks were due to environments differing in polarity, two separate peaks would appear in the $\Delta\Delta G°$ histogram.

In contrast to the $\Delta\Delta G°$ data, the λ_{oi} histogram for PMMA (see Figure 6) clearly shows two distinct peaks. Again, λ_{oi} describes the extent to which the dipoles surrounding a given molecule can move (or reorient) on a time scale similar to the excited-state lifetime, and hence, is a measure of environmental rigidity. The presence of the two peaks in the λ_{oi} histogram indicates then that the associated environments differ primarily in rigidity. One may be concluded to be more rigid and the

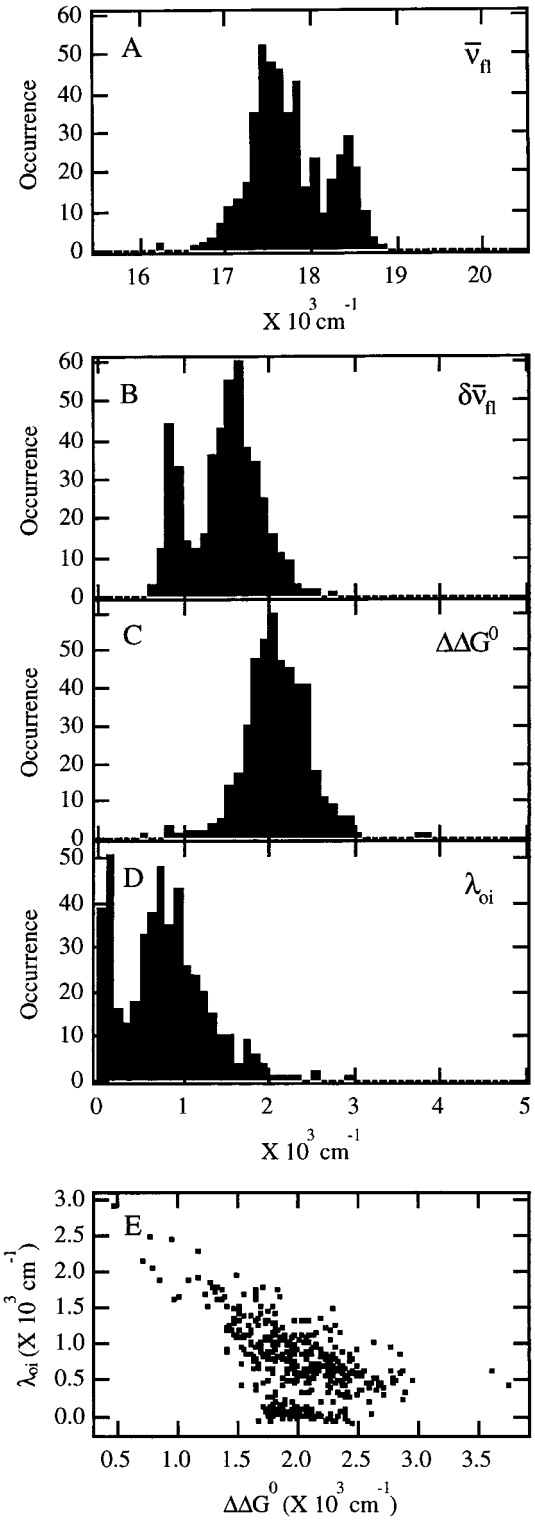

Figure 6. (A,B) Histograms of $\bar{\nu}_{fl}$ and $\delta\bar{\nu}_{fl}$ for Nile Red in a PMMA film. Peak positions and widths were measured by fitting the blue edge only of each spectrum to a Gaussian function. (C,D) Histograms of $\Delta\Delta G°$ and λ_{oi} determined from (A), (B), and curve fits of the data in Figure 2 using the equations given in the text. The two peaks observed in the $\bar{\nu}_{fl}$ and $\delta\bar{\nu}_{abs}$ data clearly indicate the presence of two separate distributions. The single and double peaks shown in the $\Delta\Delta G°$ and λ_{oi} plots, respectively, suggest the origins of the two peaks are due to variations in the dynamic properties of the local environment. (E) Correlation plot for the λ_{oi} and $\Delta\Delta G°$ data, indicating those molecules exhibiting small λ_{oi} values exhibit a range of $\Delta\Delta G°$ values similar to that exhibited by the majority of other molecules.

other more fluid in nature. Such differences may result from the presence of semicrystalline and glassy regions within the film. The differences observed between the $\Delta\Delta G°$ and λ_{oi} distributions more clearly support this conclusion than is initially apparent. While both are highly sensitive to variations in the properties of the medium, $\Delta\Delta G°$ depends on the larger $\Delta(\mu^2)$ parameter while λ_{oi} depends on $(\Delta\mu)^2$. Therefore, $\Delta\Delta G°$ should be more sensitive than λ_{oi} to variations in local properties. The appearance of a single peak in the $\Delta\Delta G°$ data is then further evidence that the two types of environments differ only in rigidity.

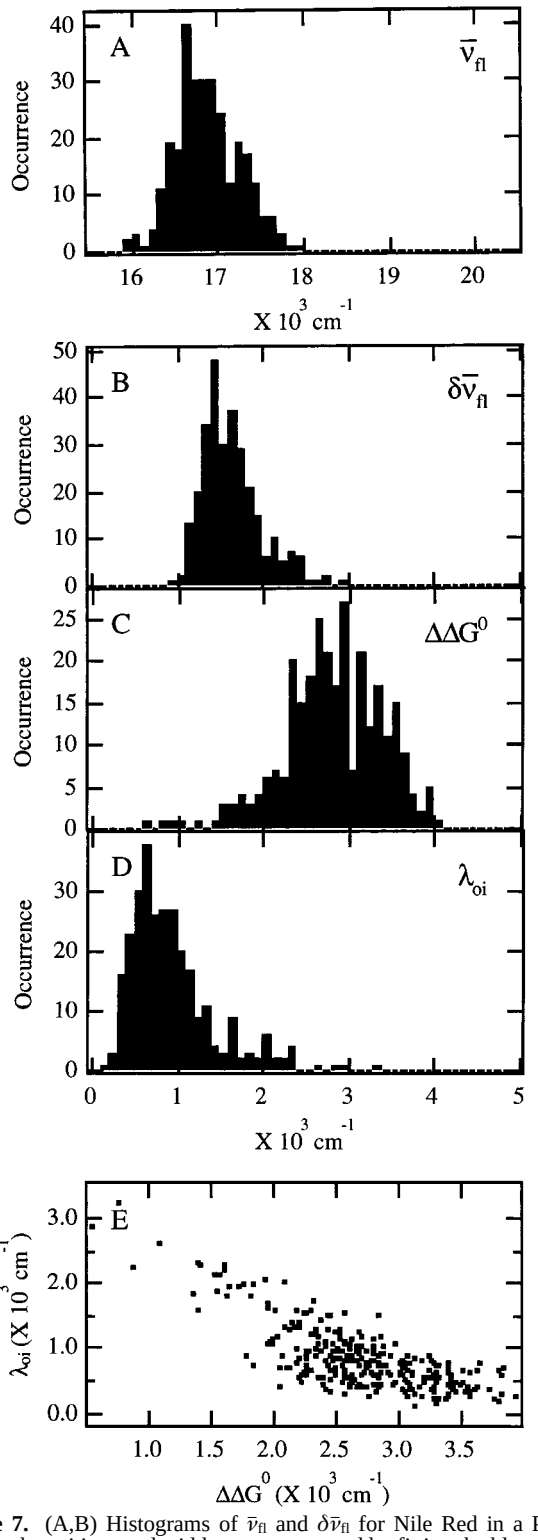

Figure 7. (A,B) Histograms of $\bar{\nu}_{fl}$ and $\delta\bar{\nu}_{fl}$ for Nile Red in a PVA film. Peak positions and widths were measured by fitting the blue edge only of each spectrum to a Gaussian function. (C,D) Histograms of $\Delta\Delta G°$ and λ_{oi} determined from (A), (B), and curve fits of the data in Figure 2 using the equations given in the text. (E) Correlation plot for the λ_{oi} and $\Delta\Delta G°$ data.

As noted earlier, the values for $\Delta\Delta G°$ and λ_{oi} used in the above analyses were determined under the assumption that λ_i is the same for each molecule. In fact, this assumption is not completely valid, as suggested by the observation of a few single molecule spectra with widths narrower than those recorded in hexane solution. Furthermore, some variability in the vibronic band spacings in the spectra published here and elsewhere[26] has been observed. These results suggest that certain molecular motions may be frozen in some environments, thus yielding different values of λ_i. The error associated with the determination of λ_{oi} is increased by this effect. However, as noted above, the spectral width data actually provides information on the total reorganization energy. Since both λ_i and λ_{oi} reflect the environmental rigidity (by different mechanisms), the conclusions remain the same, regardless of the exact mechanism (associated with the reorganization energy) of spectral broadening.

The extent to which spectral diffusion phenomena contribute to the observed width was also explored. In these experiments, the single molecule fluorescence spectra were recorded over much shorter time scales (0.25 s integration times). Tens of spectra were usually obtained before the molecules bleached. These data show that spectral diffusion on >0.25 s time scales contributes on average, ≈ 200 cm^{-1} of width to the spectra. These results are consistent with previously published work.[24] Low-temperature studies of spectral diffusion by hole burning,[47] and single molecule methods,[17,47] show even smaller effects. In contrast, time-resolved studies of similar molecules in confined systems (i.e., micelles)[56] show that spectral shifts due to solvent reorganization during the excited-state lifetime are several times larger. Indeed, the contributions of spectral diffusion noted here are small in comparison to the vast majority of single molecule spectral widths, which are found in the $1200-2000$ cm^{-1} range (see Figures 6 and 7). While these arguments may not prove spectral diffusion is negligible in the present experiments, they provide valuable evidence that the contributions of λ_{oi} to the spectral width are dominant.

Further evidence that the two peaks in the $\bar{\nu}_{fl}$ and $\delta\bar{\nu}_{fl}$ data arise from variations in environmental rigidity alone is deduced from the lack of a clear correlation between the λ_{oi} and $\Delta\Delta G°$ data. Figure 6 shows a plot of the λ_{oi} values, versus their respective $\Delta\Delta G°$ values. As is readily apparent, the molecules exhibiting the smallest λ_{oi} values exhibit approximately the same range in $\Delta\Delta G°$ as the vast majority of other molecules. Therefore, it may again be concluded that the proposed rigid and fluid environments have, on average, similar polarities. For molecules exhibiting larger λ_{oi} values (see Figures 6 and 7), a negative correlation with $\Delta\Delta G°$ appears to exist. This result is opposite of that expected from the continuum model described above. Although the exact origins of the negative correlation are unknown, it is believed to simply reflect the limitations of the continuum model, which neglect specific chemical interactions. The negative correlation may then depict the effects of these interactions (i.e., such as hydrogen bonding in the PVA film) which, in the most polar environments (having larger $\Delta\Delta G°$ values) may constrict molecular motions (yielding smaller λ_{oi} values).

Additional observations on the nature of the environments found in these films may be made from the histograms shown in Figures 6 and 7. To aid interpretation, these distributions were fit to Gaussian functions. Table 1 presents the relevant fitting parameters. Gaussian functions were selected for this procedure, based on the assumption that random distributions of environments exist in these materials. Some of the PVA histograms incorporate a long tail and can only be fit approximately.

TABLE 1: Results from Gaussian Fits to the Data Shown in Figures 6 and 7[a]

	$\bar{\nu}_{fl}$ max (fwhm)	$\delta\bar{\nu}_{fl}$ max (fwhm)	$\Delta\Delta G°$ (fwhm)	λ_{oi} (fwhm)
PMMA (1)	18400 (400)	840 (180)	2000 (770)	100 (170)
PMMA (2)	17500 (680)	1600 (570)	NA (NA)	770 (760)
PVA (dry)	16800 (860)	1500 (630)	2800 (1300)	700 (740)
PVA (fresh)	16500 (620)	1700 (620)	3000 (1400)	870 (1400)

[a] The peak positions and fwhm (in parentheses) for each Gaussian are given. The PMMA data were fit to two separate Gaussians in all but the case of $\Delta\Delta G°$. All parameters are in cm^{-1}.

Clearly, the PMMA spectra are shifted well to the blue of the PVA spectra, as shown in the $\bar{\nu}_{fl}$ and $\Delta\Delta G°$ data. This is the expected result since PMMA is less polar than PVA. In contrast, the distributions in the spectral width and λ_{oi} data are very similar for dry PVA and the larger of the two PMMA peaks. These similarities were not initially expected. The much lower polarity of PMMA suggests λ_{oi} should be smaller on average than for PVA. This result suggests that the dry PVA environments are more rigid than the majority of PMMA environments. Extensive cross-linking via hydrogen bonding in PVA may explain this observation. A minority of the PMMA environments (e.g., the second peak) do, however, exhibit greater rigidity than PVA. Again, these regions may be semicrystalline in nature. It is also clear from the data in Table 1 that the dry PVA $\Delta\Delta G°$ distribution is much broader than in PMMA. This observation indicates that the dry PVA film incorporates a much wider range of environments of different polarities and is therefore much more inhomogeneous. This is to be expected for highly polar materials where the relatively strong local dipoles can assume a range of orientations, yielding environments with properties varying from highly nonpolar to very polar.

To determine the extent to which residual solvent contributes to the above effects, the single molecule experiments were performed for both fresh and dry samples of PMMA and PVA. Fresh samples were prepared and used immediately. Data from dry PMMA films were collected after allowing the samples to dry under ambient conditions for at least 24 h. Dry PVA samples were dried for at least 2 h under a nitrogen atmosphere and imaged under similar conditions. No significant differences were observed between the fresh and dry PMMA distributions. In contrast, the PVA samples showed noticeable differences. Distributions for the fresh PVA films (like those shown in Figure 7) were approximately fit to Gaussian functions; the results are given in Table 1. Only single-peaked distributions were obtained, indicating that the two peaks observed in the PMMA data were not likely caused by the presence of residual solvent. However, as shown in Table 1, the single molecule spectra obtained in the fresh PVA samples were noticeably broader than those of the dry films. In addition, much greater variability in the measured spectral widths for the fresh samples was observed (i.e., the $\delta\bar{\nu}_{fl}$ distribution is broader). As a result, the distribution in λ_{oi} is shifted to larger values and is also broader for the fresh PVA samples. This result indicates the environments in the fresh films are more fluid and perhaps more polar in nature. In contrast, the $\Delta\Delta G°$ distribution for the fresh sample is much narrower and is shifted slightly to larger values. These results indicate that the fresh films are more homogeneous and also more polar. From these results, it may be concluded that the fresh films contain significant quantities of water; the residual water plays a significant role in determining the properties of the local environments.

Finally, it should be noted that the fluorescence images recorded for fresh PVA films differed markedly in appearance from those recorded for PMMA and dry PVA films. In contrast

to the solid, round fluorescent spots observed in the images of the latter, images of fresh PVA films showed a large number of "streaks", as depicted in Figure 4. To help determine the origins of these streaks, the spectrally integrated, time-dependent fluorescence signal was recorded for numerous single molecules. All samples showed "blinking" or "switching" behavior on several different time scales. Rapid blinking observed on the ≈1 ms time scale is attributed here to triplet blinking.[25] Blinking observed on much longer time scales (seconds) was also observed, primarily in fresh PVA films. This type of blinking is believed to cause the image streaks. The differences between the fresh and dry PVA and PMMA samples are proposed to reflect differences in local environmental properties. Specifically, they are concluded to be due to the presence of residual water in the fresh PVA samples. Photochemical reaction with oxygen could cause similar blinking via a quenching mechanism. However, since the PMMA and fresh PVA films were studied under similar ambient conditions, this possibility may be rejected as the major cause of the blinking and streaks seen in fresh PVA.

The apparent sensitivity of the blinking phenomenon to water content is likely related to solvent-dependent variations in the efficiency of TICT state formation. In polar, hydrated PVA environments, formation of the TICT state is enhanced via a reduction in the energetic barrier between ICT and TICT states, as has been shown for similar molecules.[57] As the environment varies spatially, or in time (i.e., via solvent diffusion), the efficiency of TICT state formation also varies. Hence, time- and solvent-dependent variations in the quantum yield for emission arise. The dramatic variations in the quantum yield of emission observed for Nile Red in different solvents supports this model.[53] In the absence of residual water (i.e., in dry PVA films), although the films remain highly polar, the rigid nature of the film environments likely increases the energetic barrier between ICT and TICT state, preventing its formation, and greatly reducing blinking and streaking. In the case of PMMA, the nonpolar nature of the material may effectively prevent TICT state formation altogether.

V. Conclusions

In summary, it has been demonstrated that single molecule spectroscopic studies of thin polymer films, using Nile Red as a probe molecule, provide new information on the properties of the local, nanometer-scale environments found within these films. Using a theoretical model for the dependence of the single molecule fluorescence spectra on their local environment, detailed information on the "static" and "dynamic" properties of these materials was obtained. The methods employed here are now being applied to technologically important materials, such as silicate glasses prepared by the sol−gel process,[35] and promise to yield a better understanding of the chemistry that occurs within these films when used in sensor applications.

Acknowledgment. The authors gratefully acknowledge the support of the National Science Foundation through NSF CAREER and instrumentation grants. The NSF-REU program is also acknowledged for its support of C.M. The authors also thank the donors of the Petroleum Research Foundation, administered by the American Chemical Society for their support.

References and Notes

(1) Seitz, W. R. *Anal. Chem.* **1984**, *56*, 16A.
(2) Dave, B. C.; Dunn, B.; Valentine, J. S.; Zink, J. I. *Anal. Chem.* **1994**, *66*, 1120A.
(3) Lev, O.; Tsionsky, M.; Rabinovich, L.; Glezer, V.; Sampath, S.; Pankratov, I.; Gun, J. *Anal. Chem.* **1995**, *67*, 22A.
(4) Soper, S. A.; Warner, I. M.; McGown, L. B. *Anal. Chem.* **1998**, *70*, 477R.
(5) Reichardt, C. *Chem. Rev.* **1994**, *94*, 2319.
(6) Dunn, B.; Zink, J. I. *Chem. Mater.* **1997**, *9*, 2280.
(7) Matsui, K.; Matsuzuka, T.; Fujita, H. *J. Phys. Chem.* **1989**, *93*, 4991.
(8) Matsui, K.; Nozawa, K. *Bull. Chem. Soc. Jpn.* **1997**, *70*, 2331.
(9) Gvishi, R.; Narang, U.; Bright, F. V.; Prasad, P. N. *Chem. Mater.* **1995**, *7*, 1703.
(10) Dutta, A. K.; Kamada, K.; Ohta, K. *J. Photchem. Photobiol. A* **1996**, *93*, 57.
(11) Lobnik, A.; Wolfbeis, O. S. *Proc. SPIE* **1997**, *3136*, 284.
(12) Chen, P.; Meyer, T. J. *Chem. Rev.* **1998**, *98*, 1439.
(13) Lakowicz, J. R. *Principles of Fluorescence Spectroscopy*; Plenum: New York, 1983.
(14) Moerner, W. E. *Science* **1994**, *265*, 46.
(15) Moerner, W. E.; Kador, L. *Phys. Rev. Lett.* **1989**, *62*, 2535.
(16) Shera, E. B.; Seitzinger, N. K.; Davis, L. M.; Keller, R. A.; Soper, S. A. *Chem. Phys. Lett.* **1990**, *174*, 553.
(17) Ambrose, W. P.; Moerner, W. E. *Nature* **1991**, *349*, 225.
(18) Betzig, E.; Chichester, R. J. *Science* **1993**, *262*, 1422.
(19) Ambrose, W. P.; Goodwin, P. M.; Martin, J. C.; Keller, R. A. *Phys. Rev. Lett.* **1994**, *72*, 160.
(20) Xie, X. S.; Dunn, R. C. *Science* **1994**, *265*, 361.
(21) Nie, S.; Chiu, D. T.; Zare, R. N. *Science* **1994**, *266*, 1018.
(22) Moerner, W. E. *Acc. Chem. Res.* **1996**, *29*, 563.
(23) Macklin, J. J.; Trautman, J. K.; Harris, T. D.; Brus, L. E. *Science* **1996**, *272*, 255.
(24) Lu, H. P.; Xie, X. S. *Nature* **1997**, *385*, 143.
(25) Ha, T.; Enderle, T.; Chemla, D. S.; Selvin, P. R.; Weiss, S. *Chem. Phys. Lett.* **1997**, *271*, 1.
(26) Weston, K. D.; Carson, P. J.; Metiu, H.; Buratto, S. K. *J. Chem. Phys.* **1998**, *109*, 7474.
(27) Dickson, R. M.; Cubitt, A. B.; Tsien, R. Y.; Moerner, W. E. *Nature* **1997**, *388*, 355.
(28) Vanden Bout, D. A.; Yip, W.-T.; Hu, D.; Fu, D.-K.; Swager, T. M.; Barbara, P. F. *Science* **1997**, *277*, 1074.
(29) Yip, W.-T.; Hu, D.; Yu, J.; Vanden Bout, D. A.; Barbara, P. F. *J. Phys. Chem. A* **1998**, *102*, 7564.
(30) Ha, T.; Glass, J.; Enderle, T.; Chemla, D. S.; Weiss, S. *Phys. Rev. Lett.* **1998**, *80*, 2093.
(31) Ha, T.; Enderle, T.; Chemla, D. S.; Selvin, P. R.; Weiss, S. *Phys. Rev. Lett.* **1996**, *77*, 3979.
(32) Dickson, R. M.; Norris, D. J.; Tzeng, Y.-L.; Moerner, W. E. *Science* **1996**, *274*, 966.
(33) Schmidt, T.; Schütz, G. J.; Baumgartner, W.; Gruber, H. J.; Schindler, H. *J. Phys. Chem.* **1995**, *99*, 17662.
(34) Schmidt, T.; Schütz, G. J.; Baumgartner, W.; Gruber, H. J.; Schindler, H. *Proc. Natl. Acad. Sci.* **1996**, *93*, 2926.
(35) Wang, H.; Bardo, A. M.; Collinson, M. M.; Higgins, D. A. *J. Phys. Chem. B* **1998**, *102*, 7231.
(36) Wirth, M. J.; Swinton, D. J. *Anal. Chem.* **1998**, *70*, 5264.
(37) Marcus, R. A. *J. Chem. Phys.* **1965**, *43*, 1261.
(38) Marcus, R. A. *J. Phys. Chem.* **1989**, *93*, 3078.
(39) Marcus, R. A. *J. Phys. Chem.* **1990**, *94*, 4963.
(40) Lippert, E. *Z. Naturforsch. A* **1955**, *10*, 541.
(41) Lippert, E. *Z. Phys. Chem.* **1956**, *6*, 125.
(42) Mataga, N.; Kaifu, Y.; Koizumi, M. *Bull. Chem. Soc. Jpn.* **1955**, *28*, 690.
(43) Mataga, N.; Kaifu, Y.; Koizumi, M. *Bull. Chem. Soc. Jpn.* **1956**, *29*, 465.
(44) Brunschwig, B. S.; Ehrenson, S.; Sutin, N. *J. Phys. Chem.* **1987**, *91*, 4714.
(45) Worl, L. A.; Meyer, T. J. *Chem. Phys. Lett.* **1988**, *143*, 541.
(46) Wrighton, M.; Morse, D. L. *J. Am. Chem. Soc.* **1974**, *96*, 998.
(47) Orrit, M.; Bernard, J.; Personov, R. I. *J. Phys. Chem.* **1993**, *97*, 10256.
(48) Pariser, R.; Parr, R. G. *J. Chem. Phys.* **1953**, *21*, 466.
(49) Pariser, R.; Parr, R. G. *J. Chem. Phys.* **1953**, *21*, 767.
(50) Pople, J. A. *Trans. Faraday Soc.* **1953**, *49*, 1375.
(51) Griffiths, J. *Dyes Pigments* **1982**, *3*, 211.
(52) Rettig, W. *Angew. Chem., Int. Ed. Engl.* **1986**, *25*, 971.
(53) Sarkar, N.; Das, K.; Nath, D. N.; Bhattacharyya, K. *Langmuir* **1994**, *10*, 326.
(54) Golini, C. M.; Williams, B. W.; Foresman, J. B. *J. Fluoresc.* **1998**, *8*, 395.
(55) Dutt, G. B.; Doraiswamy, S.; Periasamy, N. *J. Chem. Phys.* **1991**, *94*, 5360.
(56) Willard, D. M.; Riter, R. E.; Levinger, N. E. *J. Am. Chem. Soc.* **1998**, *120*, 4151.
(57) Jones, G.; Jackson, W. R.; Choi, C.; Bergmark, W. R. *J. Phys. Chem.* **1985**, *89*, 294.